Atmospheric
Measurement
Techniques

The "dual-spot" Aethalometer: an improved measurement of aerosol black carbon with real-time loading compensation

L. Drinovec[1], G. Močnik[1], P. Zotter[2,*], A. S. H. Prévôt[2], C. Ruckstuhl[3], E. Coz[4], M. Rupakheti[5], J. Sciare[6], T. Müller[7], A. Wiedensohler[7], and A. D. A. Hansen[1,8]

[1]Aerosol d.o.o., 1000 Ljubljana, Slovenia
[2]Paul Scherrer Institute, 5232 Villigen, Switzerland
[3]inNET Monitoring AG, 6460 Altdorf, Switzerland
[4]Centro de Investigaciones Energéticas, Medioambientales y Tecnológicas, 28040 Madrid, Spain
[5]Institute for Advanced Sustainability Studies, 14467 Potsdam, Germany
[6]Laboratoire du Climat et de l'Environnement, CEA/Orme des Merisiers, 91191 Gif-sur-Yvette, France
[7]Leibniz Institute for Tropospheric Research, 04318 Leipzig, Germany
[8]Magee Scientific Corp., Berkeley, California, CA 94703, USA
[*]now at: Lucerne School of Engineering and Architecture, Bioenergy Research, Lucerne University of Applied Sciences and Arts, Horw 6048, Switzerland

Correspondence to: L. Drinovec (luka.drinovec@aerosol.si) and G. Močnik (grisa.mocnik@aerosol.si)

Abstract. Aerosol black carbon is a unique primary tracer for combustion emissions. It affects the optical properties of the atmosphere and is recognized as the second most important anthropogenic forcing agent for climate change. It is the primary tracer for adverse health effects caused by air pollution. For the accurate determination of mass equivalent black carbon concentrations in the air and for source apportionment of the concentrations, optical measurements by filter-based absorption photometers must take into account the "filter loading effect". We present a new real-time loading effect compensation algorithm based on a two parallel spot measurement of optical absorption. This algorithm has been incorporated into the new Aethalometer model AE33. Intercomparison studies show excellent reproducibility of the AE33 measurements and very good agreement with post-processed data obtained using earlier Aethalometer models and other filter-based absorption photometers. The real-time loading effect compensation algorithm provides the high-quality data necessary for real-time source apportionment and for determination of the temporal variation of the compensation parameter k.

1 Introduction

The combustion of carbonaceous fuels inevitably results in the emission of gas and particulate air pollutants. One of the fractions of the emitted particles are light-absorbing carbonaceous aerosol compounds, in particular black carbon (BC), an aerosol species exhibiting very large optical absorption across the visible part of the optical spectrum. Black carbon is a unique primary tracer for combustion emissions as it has no non-combustion sources. It is inert and can be transported over great distances (Hansen et al., 1989; Bodhaine, 1995; Sciare et al., 2009). Black carbon affects the optical properties of the atmosphere when suspended and is recognized as the second most important anthropogenic forcing agent for climate change after CO_2 (Ramanathan and Carmichael, 2008; Bond et al., 2013). Black carbon is also the leading indicator of the adverse health effects caused by particulate air pollution (Janssen et al., 2011, 2012; Grahame et al., 2014). Reducing air pollution is a major societal need, which must be addressed at a local, national, regional and global scale. Source apportionment of air pollutants and determination of the time evolution of the source contributions to their ambient concentrations are essential for these efforts. Black car-

Table 1. Model equations describing the filter loading effect.

Weingartner et al. (2003)	$BC = \dfrac{BC_{NC}}{\left(\frac{1}{f}-1\right)\cdot\left(\frac{\ln(ATN)-\ln(10)}{\ln(50)-\ln(10)}\right)+1}$
Virkkula et al. (2007)	$BC = BC_{NC} \cdot (1 + k \cdot ATN)$

bon as a primary pollutant, closely related to sources, must be measured.

Optical methods are used for real-time determination of aerosol black carbon concentrations. The sample air stream is drawn through a filter tape, and the aerosol particles are collected on it. Optical filter photometers perform measurements of light transmission (Hansen et al., 1982, 1984; Bond et al., 1999) or a combination of reflection and transmission measurements (Petzold et al., 2005). Transmission of light through the sample-laden filter is measured and the attenuation (ATN) coefficient is calculated from the rate of attenuation change with time. The attenuation coefficient is converted to the absorption coefficient, and the mass equivalent black carbon concentration (Petzold et al., 2013) is calculated by dividing the absorption coefficient with the BC specific mass absorption cross section. Other methods to determine the absorbing and/or refractory and/or thermally stable carbonaceous aerosol include photo-acoustic detection, light-induced incandescence and thermal–optical analysis (Arnott et al., 1999; Stephens et al., 2003; Chow et al., 1993; Birch and Cary, 1996; Cavalli et al., 2010).

All filter-based optical methods exhibit loading effects (Bond et al., 1999; Weingartner et al., 2003; Virkkula, 2010; Virkkula et al., 2005, 2007; Collaud Coen et al., 2010; Park et al., 2010; Hyvärinen et al., 2013). The relationship between attenuation and BC surface loading is linear for low attenuation values. However, this relationship becomes nonlinear when the attenuation values are high due to a filter saturation effect (Gundel et al., 1984). In the presence of saturation, assuming linear proportionality between attenuation and the BC surface loading would lead to underestimation of the BC concentrations. The measurements must be compensated for this loading effect, so that they accurately represent the ambient BC concentrations. This has been performed in the past with an algorithm embedded in the filter photometer, assuming fixed compensation parameters (Bond et al., 1999; Virkkula, 2010; Virkkula et al., 2005, 2007) or with an attempt to compensate the data by performing an additional measurement of reflection (Petzold and Schönlinner, 2004) or scattering (Arnott et al., 2005). Alternatively, a post-processing algorithm can be employed using either fixed parameters (Hyvärinen et al., 2013) or parameters obtained from the data themselves (Virkkula et al., 2007; Park et al., 2010; Hyvärinen et al., 2013). Weingartner et al. (2003) and Virkkula et al. (2007) models have been most frequently used for loading effect compensation of the Aethalometer data (Table 1). The non-compensated concentration, BC_{NC}, reported by the instrument is compensated
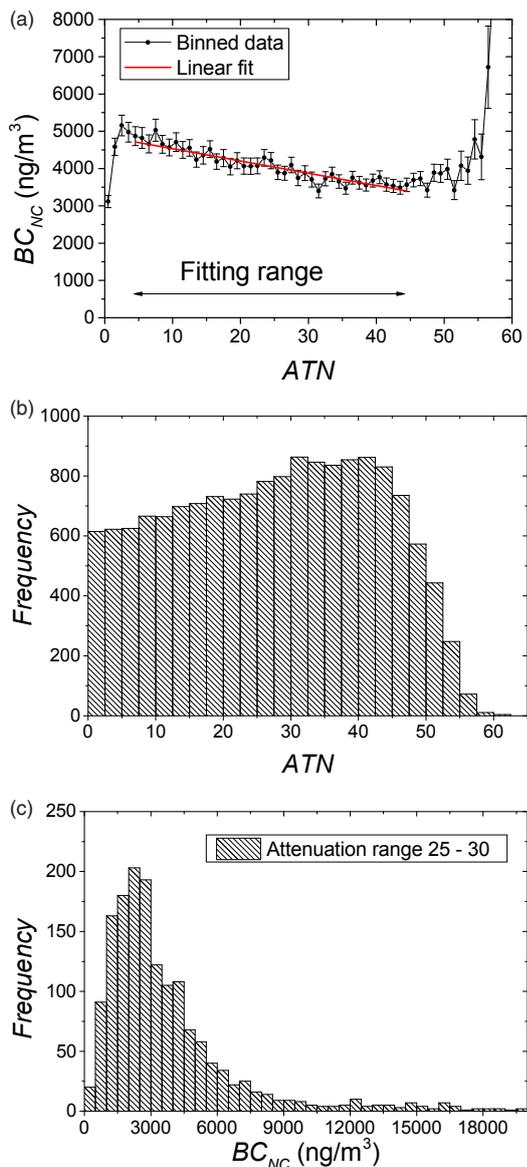
using a pre-determined compensation parameter (f or k depending on the model) and the attenuation values, as measured by the Aethalometer, to determine the compensated BC concentration.

Post-processing the data allows determination of slowly changing compensation parameters which are representative for a longer measurement period. However, it has been shown that the loading effect differs between the seasons, depending on the aerosol properties (Virkkula et al., 2007). Weingartner et al. (2003) have shown that fresh aerosols exhibit more pronounced loading effects than aged ones. The assumption of fixed or specified aerosol properties will introduce systematic errors in the data when the assumed values are incorrect for the sampled aerosol. Especially aerosols from local sources exhibit great temporal and spatial variability and these variations need to be addressed in the algorithms to accurately compensate the data. Post-processing eliminates the loading effects in the data but it frequently relies upon assumptions of the compensation parameters. It also requires time and resources for data processing. The compensation parameters depend on the wavelength of light used in the analysis (Weingartner et al., 2003). Accurate compensation of absorption measurements is essential if the spectral measurements are used for source apportionment of BC or carbonaceous aerosols (Sandradewi et al., 2008b).

Therefore, it is absolutely crucial that the compensation is validated. In filter photometers, there is an automatic tape change when an attenuation threshold is reached. Thus, one can observe a discontinuity of BC when transitioning from a loaded spot to a fresh one, where loading effects are negligible. Providing that the concentration does not change in the time, during which the filter tape is being advanced (typically 20 min), these discontinuities in the BC concentration at the time of the tape advance display the "goodness" of the compensation. A simpler method, making no assumptions, follows the method described in Park et al. (2010) and is developed into a criterion for the test of the compensation in Segura et al. (2014), examining the nonlinearity by plotting the dependence of the measured BC on the accumulated surface loading on the filter as reported by the measured optical attenuation.

A solution, which is superior to the compensation methods described above, is to measure the nonlinearity with high time resolution by the filter photometer itself. First, we start by introducing the loading effect and the method to measure it from the non-compensated data. Then we describe an approach to show how to measure the loading effect. This is achieved by measuring the attenuation of light on two sam-

Mode	Valve 1	Valve 2	Valve 3	Valve 4
Bypass	1	1	0	1
Warm-up / clean air	0	0	1	1
Measurement	0	0	0	0
Flowmeter calibration	0	1	0	0

Figure 1. The AE33 flow diagram. During measurement, the inlet air passes through filter spots S1 and S2, each with a different flow rate, as set by the orifice 2. Airflow through S1 is measured by the mass flowmeter 1; flow through S2 is calculated as a difference between the total flow (flowmeter C) and flow through S1. The valves are used for routing of airflow during different modes of operation (see the table above). The bypass mode is used during the tape advance procedure with orifice 1 mimicking the filter flow resistance.

ple spots with different loading and using this information to extrapolate the measurements to zero loading, thereby eliminating the nonlinearity. We introduce the new Aethalometer model AE33 that performs such a measurement and compensates for the nonlinearity in real time.

2 Methods

The new Aethalometer model AE33 collects aerosol particles on the filter continuously by drawing air containing the aerosol through the filter tape. It measures the transmission of light through the filter tape containing the sample and through an unloaded part (spot) of the filter tape acting as a reference area, at seven different wavelengths. It deduces the optical properties and the instantaneous concentration from the rate of change of the attenuation of light in the particle-laden filter. In the newly developed Aethalometer, two measurements are obtained simultaneously from two sample spots with different rates of accumulation of the sample. Both spots derive their samples from the same input air stream. Consequently, any nonlinearity will have the same fundamental characteristics, but the resulting saturation will be of different magnitude. The two results are then combined to eliminate nonlinearities and provide the compensated particle light absorption and BC mass concentration. The method explicitly does not require any knowledge or assumption about the existence, origin or magnitude of the nonlinearity arising from the properties of the aerosol particles collected on the filter.

2.1 Aethalometer AE33

The newly developed Aethalometer model AE33 (Magee Scientific) follows the same basic measurement principle as the older models. Aerosol particles are continually sampled on the filter and the optical attenuation is measured with high time resolution 1 s or 1 min. Attenuation is measured on two spots with different sample flows and on the reference spot without the flow (Fig. 1). The BC mass concentration is calculated from the change in optical attenuation at 880 nm in the selected time interval using the mass absorption cross section $7.77\,\mathrm{m^2\,g^{-1}}$. At this wavelength, other aerosol particles (carbonaceous or mineral) absorb significantly less and absorption can be attributed to BC alone (Sandradewi et al., 2008a and b; Fialho et al., 2005; Yang et al., 2009; and references therein). Measurements at distinct spectral regions (370, 470, 520, 590, 660, 880 and 950 nm) allow for spectral analysis of the data – the analysis of the dependence of absorption on the wavelength can be of importance for research on direct effects of aerosol BC, climate forcing (Bond et al., 2013; IPCC, 2013) or mineral dust detection (Collaud Coen et al., 2004), through the determination of the single scattering albedo dependence on the wavelength, or source apportionment (Sandradewi et al., 2008b).

When the attenuation reaches a certain threshold, a tape advance is induced so that measurements start on a clean spot. The attenuation threshold, first reached at the lowest wavelength 370 nm, is called $\mathrm{ATN_{TA}}$ (see Eq. (1) in Sect. 2.3

Figure 2. Example of the analysis of the filter loading effect: BC as a function of ATN. **(a)** BC(ATN) plot: a linear least squares regression in the ATN range 5–45 was used to fit the data. The apparent increase in the plot at ATN = 60 is a statistical artifact. **(b)** Frequency distribution of the number of measurements per ATN bin. **(c)** The BC frequency distribution in the bin $25 < \text{ATN} < 30$. The measurements were performed in Klagenfurt (Austria) from 1 to 12 March 2012.

below) with a default value of 120, which can be changed by the user – for example to conserve the filter tape by setting the value larger. However, setting the ATN_{TA} value too high would impact the measurement and make it excessively noisy at high attenuation. The airflow is measured by two mass flowmeters after the aerosol particles are deposited on the filter. The flow can be reported at ambient conditions, conditions set by the users or different standard conditions,

the default being 20.11 °C and 1013.25 hPa. Several valves are incorporated in the manifold to allow for bypass (air is not flowing through the filter during tape advance procedure), clean air (air is filtered before reaching the optical chamber – used during the warm-up procedure and during automated quality control tests) and measurement modes. The flow diagram describing different flow modes can be seen in Fig. 1.

2.2 Filter material

Two different filter tape materials were tested in the new Aethalometer. Both are composed of filtering fibers attached to the polyester backing. The quartz filter is the same as used in the older Aethalometer types (Pallflex Q250F) and tetrafluoroethylene (TFE)-coated glass filter (Pallflex "Fiberfilm" T60A20). Different filter types influence the loading effect and the multiple scattering in the filter matrix differently. The main reason to introduce a TFE-coated glass filter is the sensitivity of the quartz filter to changes in sample air stream humidity. While the Global Atmospheric Watch recommendation states that aerosol optical properties should be measured at low and stable relative humidity (WMO/GAW, 2003), many instruments for measurement of aerosol absorption and scattering are operated without them.

2.3 Evaluation method for loading effect compensation algorithms

The attenuation of light in the filter tape loaded with the sample is calculated as

$$\text{ATN} = -100 \cdot \ln \left(I \, / \, I_0 \right), \tag{1}$$

where I is the detector intensity signal for the measurement spot and I_0 the detector signal for the reference spot. The factor 100 is there for convenience only (Gundel et al., 1984). The loading effect was analyzed using a plot of the BC dependence on attenuation (Park et al., 2010; Segura et al., 2014). This approach is based on the idea that within a long enough measurement campaign the probability to measure a certain BC value in an ATN bin is constant and independent of the ATN:

$$\text{BC}\,(\text{ATN}) = \overline{\text{BC}}. \tag{2}$$

However, the presence of the loading effect in filter-based absorption photometers causes an ATN-dependent change in the instrumental sensitivity. In the Aethalometers, this is seen as the reduction of measured BC at higher attenuations (Fig. 2a). For the quantitative analysis, low values of attenuation are omitted because of the transients after tape advances. At attenuations above a certain value, the frequency of measurements drops (Fig. 2b) and the assumption of Eq. (2) does not hold any more (for example, tape advances may be triggered by high BC events). Consequently, data with ATN > 45 in Fig. 2a are not used for fitting the dependence of the instrumental sensitivity as the function of ATN.
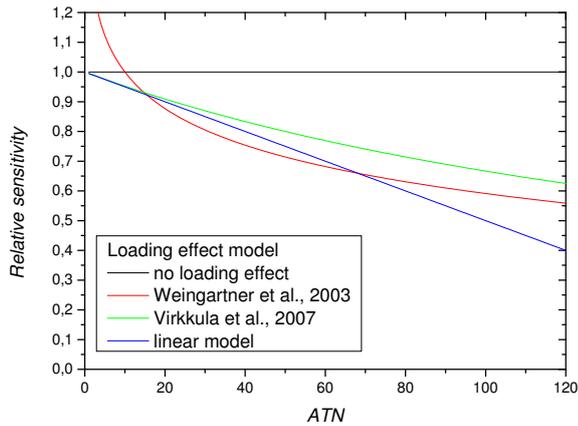
Figure 3. Comparison of the filter loading effect models. The Weingartner et al. (2003) model curve (Table 1) was calculated using $f = 1.4$; for the Virkkula et al. (2007) approach (Table 1) and the proposed dual-spot compensation model (Eq. 6), $k = 0.005$ was used.

In Aethalometers, BC(ATN) can be well approximated using a linear fit (Fig. 2a), in which the average concentration in the analyzed period (BC_0) is the intercept and RS is the relative slope of the instrumental sensitivity:

$$BC(ATN) = BC_0 + \frac{dBC}{dATN} \cdot ATN = BC_0 (1 + RS \cdot ATN), \tag{3}$$

$$RS = \frac{1}{BC_0} \frac{dBC}{dATN}. \tag{4}$$

This approach can be applied for any measurement parameter, for example the optical absorption coefficients $b_{abs}(\lambda)$ or the optical absorption Ångström exponent α (Ångström, 1929). Care should be taken that the frequency distribution within the respective ATN bins is mono-modal (Fig. 2c). This validates the use of a single period for analysis, as the aerosols investigated during the period should be homogeneous – for example, the source composition should not change completely, and specific episodes (such as Saharan dust events) should be excluded. A bi-modal frequency distribution usually means that the period is composed of two distinct and different sub-periods which should be analyzed separately.

2.4 Dual-spot loading compensation algorithm

It was shown that the filter loading effect changes with location and time of the year (Virkkula et al., 2007). The BC(ATN) analysis, performed on data from five sites across the globe, shows significantly different values of the loading effect relative slope (Figs. S1–S5 and Table S1 in the Supplement). For the development of the real-time compensation algorithm, which will be applicable to aerosol particles

with different optical properties, the loading effect must be measured and parameterized with the same time resolution as the measurement itself. Herein, we describe a dual-spot approach, where the data from two filter spots with different loading are used to measure the loading effect, calculate the compensation parameter and apply it to the data to obtain compensated results.

Gundel et al. (1984) showed that the optical attenuation measured at 633 nm (Rosen et al., 1978) for samples collected on quartz filter started to deviate from the linear relationship as a function of surface loading (B) above $10 \, \mu g \, cm^{-2}$ of black carbon. This can be parameterized by an empirical relationship of ATN vs. B:

$$ATN = \frac{1}{k} \left(1 - e^{-kB\sigma} \right), \tag{5}$$

where σ is the black carbon mass attenuation cross section and k is the loading effect parameter. When particles from the sample air stream are continuously collected on the filter, the measured BC concentration is proportional to the rate of change of the filter B:

$$BC = (dB / dt) \cdot S/F, \tag{6}$$

where F is the volumetric flow and S is filter surface area on which the aerosol particles are deposited. Combining these equations we obtain

$$BC = \frac{dATN}{dt} \cdot \frac{S}{F} \cdot \frac{1}{\sigma} \cdot \frac{1}{(1 - k \cdot ATN)}$$
$$= BC_{NC} / (1 - k \cdot ATN), \tag{7}$$

where BC_{NC} represents the non-compensated black carbon concentration. This equation is similar (but not the same) to the one presented by Virkkula et al. (2007) (Table 1). In fact, expanding Eq. (6) gives a geometric series, which, in the zero and first order, gives the same dependence of the non-compensated black carbon concentration BC_{NC} on ATN as the one described by Virkkula et al. (2007). The filter loading effect (that is, the loss of sensitivity of the measurement with the loading of the filter spot) as described by different models is presented in Fig. 3.

The loading effect is a cumulative property of the cumulative deposit of particle material on the filter rather than the instantaneous black carbon concentration. Consequently, it has to be calculated from the total filter loading B and not BC (t). For two filter spots, which collect the same aerosol with different rate, we obtain different loading but the same value of the loading parameter k:

$$e^{-\sigma k B_1} = (1 - k \cdot ATN_1), \tag{8}$$

$$e^{-\sigma k B_2} = (1 - k \cdot ATN_2). \tag{9}$$

The attenuations ATN_1 and ATN_2 are measured. The filter loading values for the two sample spots B_1 and B_2 are proportional to the airflows through the two sample spots. The parameter k is determined by numerically solving the following equation:

$$y = \frac{F_2}{F_1} = \frac{\ln(1 - k \cdot ATN_2)}{\ln(1 - k \cdot ATN_1)}. \tag{10}$$

Fine tuning of the compensation algorithm

The calculation of k is very sensitive to small errors in determination of flow face velocities for both filter spots. The face velocity ratio factor (FVRF) is introduced as an additional empirical factor in the Eq. (10):

$$y = \frac{F_2}{F_1} \cdot FVRF. \tag{11}$$

FVRF is determined from the ATN_2 / ATN_1 ratio obtained at low filter loadings. A comprehensive analysis on the sensitivity of the determination of k and the determination of FVRF can be found in the Supplement (Determination of the face velocity ratio factor (FVRF); Figs. S6 and S7). In practice, FVRF is determined as an intercept of the ratio ATN_2 / ATN_1 vs. ATN_1 for data fitted with the linear function within a certain attenuation range between the values ATN_{f1}; ATN_{f2}:

$$FVRF = \left(\frac{ATN_2}{ATN_1}\right)_0 \cdot \frac{F_1}{F_2}. \tag{12}$$

Choosing a lower limit on the attenuation range, ATN_{f1} is needed to avoid filter matrix transients after the tape advance. The upper limit ATN_{f2} is set to be small enough not to be influenced by the filter loading effect (compare with ranges shown in Fig. 2). FVRF is calculated from data at low attenuations, while the determination of k is more accurate at high attenuations. For the compensation, we thus use a weighting method in which the previously determined k from the fully loaded spot before the tape advance is taken into account (see also in the Supplement under "Weighting method for loading effect compensation parameter k"; Fig. S8):

$$k_{weighted} = \frac{(ATN_{TA} - ATN_1) \cdot k_{old} + (ATN_1 - ATN_{f2}) \cdot k}{(ATN_{TA} - ATN_{f2})}, \tag{13}$$

where ATN_{TA} is the attenuation setting to trigger the tape advance (typically around 120 at 370 nm). A weighted value of the parameter k ($k_{weighted}$) is used for loading effect compensation.

2.5 Black carbon concentration calculation

The calculation of BC is based on Eq. (6). Because the airflow is measured after the air passes the filter, lateral airflow in the filter matrix under the optical chamber ζ has to be taken into account:

$$F_{in} = F_{out} \cdot (1 - \zeta). \tag{14}$$

The value of ζ is determined by measuring of input and output flow and was found to be in the 0.02–0.07 range. The optical absorption of aerosols on the filter is influenced by scattering of light within the filter – the enhancement of optical absorption is described by the factor C (Weingartner et al., 2003), which depends on the filter material:

$$b_{ATN} = C \cdot b_{abs}, \tag{15}$$

where b_{ATN} is the optical attenuation coefficient measured for aerosol particles captured on the filter while b_{abs} is the in situ absorption of aerosol particles suspended in the air. The enhancement parameter C has no statistically significant spectral dependence (Weingartner et al., 2003; Segura et al., 2014), with its value determined by comparing different methods and instruments in laboratories and in ambient observatories (Weingartner et al., 2003; Collaud Coen et al., 2010; Müller et al., 2011a; Segura et al., 2014), resulting in a range of values. The value of C may depend on the particle properties, as shown for the particle soot absorption photometer (PSAP) (Nakayama et al., 2010). It turns out that the value of C strongly depends on the filter material used (see Sect. 3.3) being $C_{quartz} = 2.14$ for quartz filter and $C_{TFE} = 1.57$ for TFE-coated glass fiber filter. BC is historically defined by Aethalometer measurement at 880 nm, so we use parameters at this wavelength to derive the mass equivalent concentration using $\sigma_{air} = 7.77 \, m^2 \, g^{-1}$, obtained initially by comparing optical and thermal measurements of filters loaded with refractory carbonaceous material (Gundel et al., 1984). We use the attenuation measured on spot 1 (the spot with the higher flow of the two spots):

$$BC = \frac{S \cdot (\Delta ATN_1 / 100)}{F_1 (1 - \zeta) \cdot \sigma_{air} \cdot C \cdot (1 - k \cdot ATN_1) \cdot \Delta t}, \tag{16}$$

where a factor of 100 is required due to the original definition of attenuation in Gundel et al. (1984). The above determination is performed simultaneously at seven different wavelengths using mass absorption cross sections listed in the Supplement (Table S2). The aerosol optical absorption coefficients are therefore

$$b_{abs}(\lambda) = \frac{S \cdot (\Delta ATN_1(\lambda) / 100)}{F_1 (1 - \zeta) \cdot C \cdot (1 - k \cdot ATN_1(\lambda)) \cdot \Delta t}. \tag{17}$$

2.6 Measurement campaigns

The dual-spot compensation algorithm was evaluated in the field during a measurement campaign in Klagenfurt (Austria) in March 2012. The performance of the new algorithm was tested for the Aethalometer model AE33 and compared to the offline compensation (Weingartner et al., 2003) used to post-process the Aethalometer model AE31 data manually.

The Klagenfurt campaign took place between 1 and 12 March 2012 at the air quality station of the Carinthian regional government at Völkermarkter Strasse, located in the middle of the busy intersection and strongly
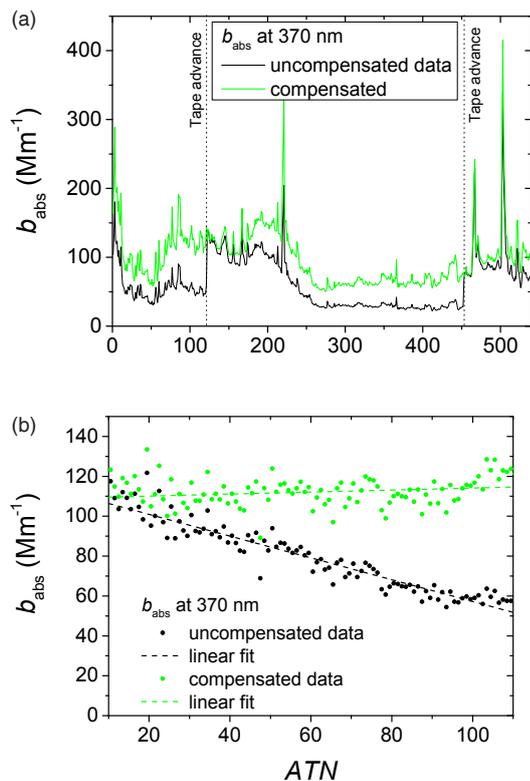
Figure 4. Comparison of the uncompensated and compensated data from the Klagenfurt campaign: **(a)** an example for b_{abs} time series measured at 370 nm comparing raw data (one spot, not compensated) and those compensated with the new algorithm for the loading effect; **(b)** $b_{abs}(ATN)$ analysis of raw and compensated data for the whole campaign. The scatter plot shows average values for each ATN bin (1 ATN unit wide). A linear least squares regression was used to fit the data and obtain the relative slope of $b_{abs}(ATN)$.

influenced by local traffic. Measurements were made using one Aethalometer model AE31 instrument (with the regular Q250 quartz filter tape) and two Aethalometer model AE33 instruments (one with the Q250 quartz filter tape, the other with T60A20 TFE-coated glass fiber filter tape) during the whole campaign. Each of the instruments was operated at an airflow of 5 L min^{-1}, with tape advances set to occur at $ATN_{TA} = 120$. The instruments were connected to a common inlet without a cyclone or a dryer. The weather during the campaign was stable (without strong wind, rain or snow). Temperatures at night were below 0 °C, and the weather was mostly sunny during the day with temperatures slightly above 0 °C. In Klagenfurt and the surrounding basin, wood is a major energy source for household heating during winter.

A set of measurements was made in Leipzig as part of the ACTRIS intercomparison workshop at TROPOS (Leibniz Institute for Tropospheric Research, Germany) from 18 to 21 February 2013 (ACTRIS, 2014a). Three Aethalometers AE33, several AE31 (average age 7 years, range 1 to

14 years), one AE22 and a MAAP (Multiangle Absorption Photometer, model 5012, Thermo Scientific) were connected to a common inlet; not necessarily all of the instruments were operational at all times during the campaign. The aerosol was dried using a silica-gel diffusion drier. During the campaign, the weather was cloudy and windy with temperatures slightly below 0 °C (ACTRIS, 2014a). The measurement site is generally considered to be moderately polluted urban background influenced by a mixture of distributed sources and some closer roads (Wehner and Wiedensohler, 2003), but the winds may have mixed the atmosphere so that the site could be representative of a broader region.

2.7 Source apportionment of black carbon emissions

Source apportionment of ambient BC concentrations is based on the Sandradewi et al. (2008b) model. Briefly, the two-component model considers the aerosol optical absorption coefficient as a sum of biomass burning and fossil fuel combustion fractions and takes advantage of the difference in the wavelength dependence of absorption: since fossil fuel and biomass contributions to aerosol absorption feature specific values of the absorption Ångström exponent, it is possible to construct a source specific two-component model. We assumed the two sources follow λ^{-1} and λ^{-2} spectral dependencies, as used in Sandradewi et al. (2008b), and Favez et al. (2010), among the range of possible values (Kirchstetter et al., 2004).

3 Results

During the Klagenfurt campaign, we observed filter loading effects in all tested Aethalometer data as expected. The effect is most pronounced for the 370 nm channel, which has highest attenuation (Fig. 4). The loading effect can be analyzed either by checking the magnitude of discontinuities at tape advances (Fig. 4a) or by performing b_{abs} as a function of ATN analysis ($b_{abs}(ATN)$ in Fig. 4b, as described in Sect. 2.3). This analysis was used to calculate relative $b_{abs}(ATN)$ slopes for all spectral channels. The same approach was used to validate the performance of the loading compensation algorithms, since the data after compensation should feature no loading effect and the relative $b_{abs}(ATN)$ slopes should be close to 0.

3.1 Compensation of AE31 data by post-processing

Data from Aethalometer AE31 were compensated manually using the Weingartner model (Weingartner et al., 2003). The compensation parameter f values were obtained by minimizing the discontinuities in b_{abs} across tape advances ($f_1 = 1.319$, $f_2 = 1.288$, $f_3 = 1.244$, $f_4 = 1.213$, $f_5 = 1.213$, $f_6 = 1.203$, $f_7 = 1.203$). As previously found (e.g., Sandradewi et al., 2008a), larger f values were obtained for shorter wavelengths although the $b_{abs}(ATN)$ method shows a somewhat smaller loading effect for that

Table 2. Summary of the characterization of the filter loading effects on the data for AE31 and AE33 (two different filter materials) during the Klagenfurt campaign. **(a)** Data were analyzed using the BC(ATN) method yielding the intercept BC_0, relative slope of BC(ATN) and the average value ($\overline{BC}$) for non-compensated (nc.) and compensated (comp.) data. Fitting parameters contain the standard error. **(b)** The same analysis was performed for the Ångström exponent α, where $\alpha = \ln(b_{470\,nm}/b_{950\,nm})/\ln(950/470)$.

(a) Instrument	BC_0 – nc. (ng m^{-3})	$\overline{BC}$ – nc. (ng m^{-3})	$\overline{BC}$ – comp. (ng m^{-3})	Relative slope BC(ATN) – nc.	Relative slope BC(ATN) – comp.
AE31	4905 ± 193	4459	4831	-0.0051 ± 0.0017	-0.0006 ± 0.0018
AE33 quartz	4909 ± 86	4379	5015	-0.0053 ± 0.0008	0.0003 ± 0.0008
AE33 TFE	4888 ± 89	4059	4960	-0.0069 ± 0.0007	-0.0003 ± 0.0008

(b) Instrument	α_0 – nc.	$\overline{\alpha}$ – nc.	$\overline{\alpha}$ – comp.	Relative slope α vs. ATN – nc.	Relative slope α vs. ATN – comp.
AE31	1.22 ± 0.01	1.07	1.29	-0.0025 ± 0.0002	-0.0010 ± 0.0002
AE33 quartz	1.26 ± 0.03	1.09	1.23	-0.0026 ± 0.0001	-0.0002 ± 0.0001
AE33 TFE	1.18 ± 0.02	0.97	1.21	-0.0033 ± 0.0003	0.0009 ± 0.0001
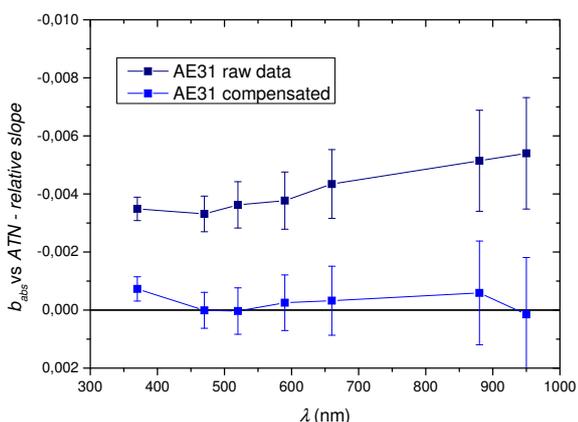
Figure 5. Filter loading effect characterization for AE31 using a quartz filter before (raw data) and after loading effect compensation during the Klagenfurt campaign. The compensation was performed using the Weingartner et al. (2003) model.

spectral range. Compensated data show small ATN dependencies (Fig. 5).

3.2 Real-time compensation of AE33 data

The real-time loading effect compensation algorithm was tested in the Aethalometer model AE33 using both the quartz Q250 and the new TFE-coated glass filter. As mentioned before, we introduced the TFE-coated glass filter to reduce changes in the sample air stream humidity which influence the correct determination of the compensation parameter k. Laboratory test results (data not shown) show that the sensitivity of TFE-coated glass filter to humidity changes is approximately 6 times smaller compared to quartz.

The real-time compensation algorithm was evaluated during the winter measurement campaign in Klagenfurt. Fig-

ure 6 shows the relative slope of b_{abs}(ATN) for uncompensated (BC determined from a single spot, as in the AE31) and compensated data for all seven wavelengths. We can observe a larger loading effect at longer wavelengths. When the data are correctly compensated, the resulting relative slope is near 0. In the AE33, we have compared the loading effect for each of the two differently loaded filter spots individually and found no statistically significant difference (-0.0069 ± 0.0007 and -0.0058 ± 0.0013).

The effectiveness of the compensation algorithm can be tested in two different ways. The first is the comparison of the parameter value at low attenuations with the campaign average for the same parameter – for example, the intersect of the BC concentration, the absorption coefficient or the absorption Ångström exponent (BC_0, b_{abs0}, α_0) in the plot showing the dependence of the parameter on ATN – to their average value. The second test is the relative slope of the tested parameter's dependence on ATN. Analysis results for AE31 with the quartz filter and AE33 with both filter types are summarized in Table 2 for BC and the Ångström exponent. As expected, the average BC is smaller than BC_0 for the non-compensated data. The difference between average BC and BC_0 is more pronounced for the TFE-coated glass fiber filter than for the quartz filter because for the same ATN, the surface loading of the filter with black carbon is larger for the TFE-coated glass fiber filter due to the smaller value of the filter matrix enhancement parameter C in this filter (see also below, Sect. 3.3). Averages of compensated data agree well with the intercept (average BC and BC_0, for example) and the differences are smaller than the standard error of the parameter. This means that the BC concentrations were well compensated. The relative slopes for BC(ATN) are almost identical and show similar loading effects for the quartz filter in both the AE31 and the AE33. For the TFE-coated glass filter, the relative slope is larger and the loading ef-
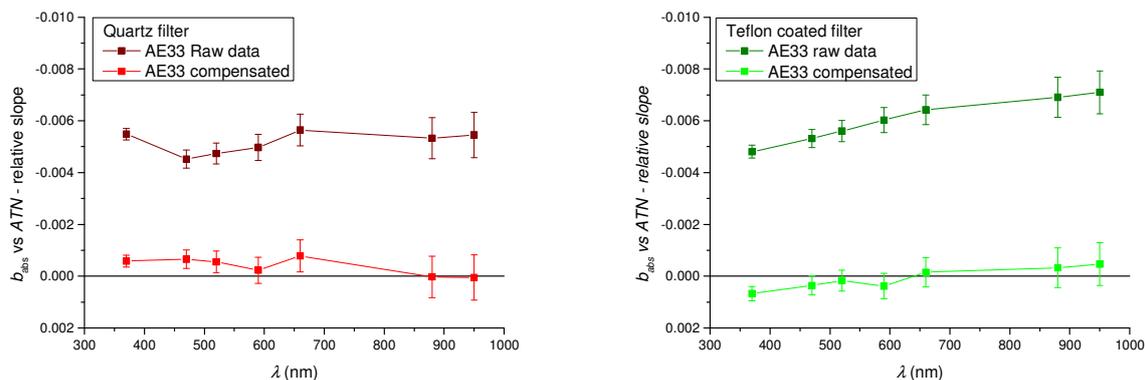
Figure 6. Filter loading effect characterization in the AE33 using quartz (left panel) and TFE-coated glass fiber filters (right panel) during the Klagenfurt campaign. The loading effect compensation was performed using the real-time dual-spot algorithm. Relative slopes of $b_{\text{abs}}(\text{ATN})$ are shown for raw and compensated data for all seven wavelengths.

fect is more pronounced. Both compensation methods work well as observed by a statistically non-significant ATN dependence of the compensated data. The maximum ATN values are different for different wavelengths and range between 120 (370 nm) and approximately 45 (950 nm).

The loading effect is stronger at lower wavelengths than at higher ones, influencing the measurement of absorption to a higher degree in blue than in the infrared (IR) part of the spectrum. The loading effect therefore reduces the determined absorption Ångström exponent α, calculated from $\alpha = \ln(b_{470\,\text{nm}}/b_{950\text{nm}})/\ln(950/470)$, as shown by the difference between the intercept α_0 and the uncompensated average value $\overline{\alpha}$ (Table 2b). Uncompensated data will not yield a correct value of α, resulting in incorrect fractions when performing black carbon source apportionment. The non-compensated average Ångström exponent lies close to 1. This value is consistent with pure diesel exhaust measured at the site. After compensation of the data, the average Ångström exponent increases to 1.21 (using Aethalometer AE33 and TFE-filter material). This change is significant, as the average BC apportioned to wood burning increases by 1 μg m^{-3} and the average BC fraction apportioned to wood burning increases from 0 to 16 % with a large diurnal variation (Fig. 9b). A similar underestimation of the contribution of wood burning would be observed in Grenoble, France, (Favez et al., 2010), and about a third lower than the actual contribution in Roveredo, Switzerland (Sandradewi et al., 2008b), if non-compensated data had been used for source apportionment of BC. The use of the compensation algorithm greatly improves the calculation of the Ångström exponent. Consequently, real-time source apportionment is possible and has been implemented in the Aethalometer model AE33.

3.3 Influence of the filter material

Measurements using the AE33 have been performed with two filter types: the quartz Q250 and the new TFE-coated

glass filter, allowing a determination of the value of the absorption enhancement parameter C. It was shown that for fresh soot particles (as expected during the Klagenfurt campaign) on quartz filter the enhancement parameter is $C \approx 2.14$ (Weingartner et al., 2003). The most robust parameter for determination of the instrument sensitivity was BC$_0$ obtained from the BC(ATN) analysis. The determination of BC$_0$ does not depend on the choice of the compensation method since the method is not employed – the parameter is determined from the uncompensated data. Parameter C for the TFE-coated glass filter was set to give the same values of BC$_0$ for both filter types. For the TFE-coated glass filter we obtained $C \approx 1.57$ using the 2-week Klagenfurt campaign data, assuming $C = 2.14$ for quartz filter (Weingartner et al., 2003). There is some uncertainty with this value since values of C for quartz filter as obtained by comparisons with other techniques differ (Weingartner et al., 2003; Collaud Coen et al., 2010; Müller et al., 2011a, Segura et al., 2014).

The parameter C influences the average loading on the filter spots since the instruments were set to advance the tape at a maximum attenuation (for the UV channel) of 120. This is the recommended maximum attenuation value, which is also the default value in the instrument but can be changed by the user to a larger or smaller value. The maximum surface loading B_{max} can be calculated using Eq. 4 and is reported in Table 3:

$$B_{\text{max}} = \frac{-\ln\left(1 - k \cdot \text{ATN}_{\text{TA}}\right)}{k \cdot \sigma_{\text{air}} \cdot C}. \tag{18}$$

The maximum surface loading should be calculated from the measured parameters in the infrared to avoid any influence of the additional absorbing compounds, such as the ones present in biomass smoke and sometimes called "Brown Carbon". These absorb heavily in the ultraviolet (UV) and blue but not in the IR part of the spectrum. By calculating the loading in the IR, absorption can be attributed to BC alone, and the surface loading can be calculated as the black carbon

Table 3. Comparison of the determined parameters for quartz and TFE-coated glass fiber filters in the AE33 (Klagenfurt campaign): k_{880} obtained from the AE33 compensation algorithm, relative slope BC(ATN) for the non-compensated data, absorption enhancement factor C and maximum filter loading B_{max} calculated at ATN (880 nm) = 50.

	k_{880}	Relative slope BC(ATN) – nc.	C	Maximum Filter loading B_{max} (μg cm^{-2})
Quartz	0.0054 ± 0.0011	-0.0053 ± 0.0008	2.14	3.5
TFE-coated glass	0.0067 ± 0.0014	-0.0069 ± 0.0007	1.57	5.0
TFE/quartz ratio (unitless)	1.24 ± 0.51	1.30 ± 0.34	1/1.36	1.43
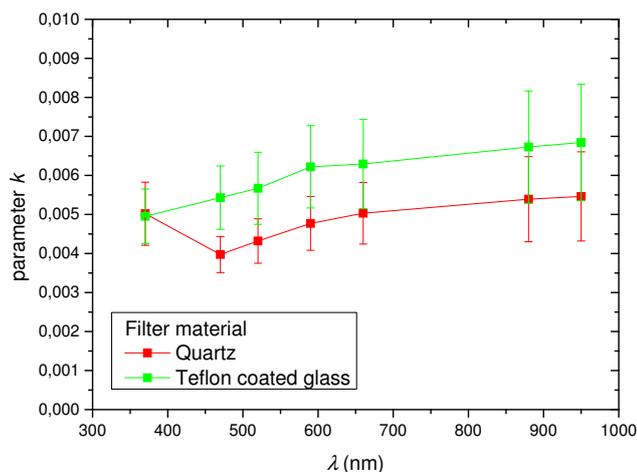
Figure 7. Comparison of the average compensation parameter $k(\lambda)$ obtained by the real-time compensation algorithm in AE33 for quartz and TFE-coated glass fiber filters during the Klagenfurt campaign.

Figure 8. Temporal variability of the compensation parameter k during the Klagenfurt campaign.

loading. In the IR, the attenuation reaches typically values around 50 for a fully loaded spot.

The maximal loading is approximately 1.43 times higher for the TFE-coated glass fiber filter, similar to the average difference in values of parameter k for both filters (1.24), indicating that the loading effect $(1 - k \times \text{ATN})$ is similar for similar filter loadings (Table 3).

A comparison of the parameter k values obtained by the real-time algorithm shows very good correlation with the relative slope of $b_{abs}(\text{ATN})$, except for the UV channel, which is hindered by transients (Fig. 7), believed to be caused by adsorption and desorption of UV-absorbing volatile organic species. These effects are more pronounced for the quartz filter.

3.4 Time dependence of parameter k

The real-time calculation of the compensation parameter k as a function of wavelength provides additional information on the physical properties of optically absorbing aerosols. Measurements during the Klagenfurt campaign show high temporal variability of this parameter (Fig. 8). There are periods with larger values of k during the night and smaller values

of k during the day. Post-processing compensation methods will produce only an average value of the compensation parameters, and therefore using a constant value of the compensation parameter for the whole campaign will cause either undercompensation or overcompensation of the data in certain time intervals.

Another advantage of using a real-time method for loading effect compensation is the possibility to perform real-time source apportionment of BC using a two-component model (Sandradewi et al., 2008b). A diurnal plot of the biomass burning contribution to BC concentration shows a trend typical for Alpine cities, where wood is used for the residential heating (compare, for example, Favez et al., 2010); there is a large contribution of biomass burning to BC concentration, with a maximum at 32 % during the night (Fig. 9). The morning peak and the onset of the afternoon peak in BC concentration are consistent with the increased traffic. The midday dip in BC is most probably caused by the thermally induced vertical mixing, because the campaign took place during the period of sunny weather. The reduction of $k_{880\,\text{nm}}$ between 9 and 15 h might be caused by the inflow of aerosols which have started to age, while the earlier reduction might be related to the change in composition, both a topic of ongoing investigations.

Table 4. The slope and r^2 of the linear least square regression through the origin of BC measurements from different filter photometers. The campaigns were conducted in Leipzig at TROPOS (ACTRIS, 2014a); Columbus, Ohio, USA (USEPA, 2014); the Aerosol d.o.o. aerosol chamber; Borgerhout, Belgium (Maetz and Peters, 2013); ZF2 ecological reserve, 55 km north of Manaus, Brazil (Holanda et al., 2014).

	Slope relative to AE33	r^2	Comparison time resolution	Test duration	Reference
AE33	1.03	0.99	5 min	2 days	ACTRIS (2014a)
	0.96	1.00	5 min		ACTRIS (2014a)
	1.06	0.99	1 h	30 days	USEPA (2014)
AE31	1.05	0.95	5 min	1 day	ACTRIS (2014a)
	0.84	0.94			ACTRIS (2014a)
	1.02	0.93			ACTRIS (2014a)
	0.93	0.92			ACTRIS (2014a)
	1.10	0.91			ACTRIS (2014a)
	1.13	0.90			ACTRIS (2014a)
AE22	0.93	0.92	5 min	1 day	ACTRIS (2014a)
	1.07	0.99	5 min	2 weeks	Chamber, this study
	0.99	0.93	1 day	3.5 months	Maetz and Peters (2013)*
MAAP	0.96	0.98	5 min	3 days	ACTRIS (2014a)
	1.07	0.97	30 min	4 months	Holanda et al. (2014)**

* Maetz and Peters (2013) compensated the AE22 data using Virkkula et al. (2007).
** Holanda et al. (2014) used an $PM_{2.5}$ inlet.

3.5 Comparison of AE33 with AE31 – the Klagenfurt field campaign

During the Klagenfurt campaign, data from the AE31 with the quartz filter and AE33 with TFE-coated glass filter were compared (Fig. 10). The AE31 data were compensated for the loading effects, using the Weingartner post-processing algorithm, while the AE33 data were compensated using the real-time "dual-spot" algorithm. The results show excellent agreement between the instruments across a wide dynamic range, with $R^2 = 0.89$, a negligible intercept of $40 \, \mathrm{ng \, m^{-3}}$ and a slope of 1.006.

3.6 Comparison of AE33 with filter photometers

During the ACTRIS campaign in Leipzig the Aethalometers AE31, AE22, AE33 and a MAAP were compared. These instruments are all filter-based absorption photometers but use different filter materials and differ in the measurement technique; Aethalometer measurements are based on the measurement of transmission of light (880 nm) through one sample spot (AE31, AE22) or two spots (AE33), whereas the MAAP uses measurement of transmission and reflection of light (637 nm) at two different angles to derive the absorption coefficient and the BC concentration using a radiative transfer model.

The instruments were compared in controlled conditions with all instruments connected to the same sampling line, using a diffusion drier. Measurements were compared with a time resolution 5 min – this is the native time resolution of the

AE31 and AE22, while AE33 and MAAP data were averaged to this resolution (ACTRIS, 2014a). The AE31 and AE22 data in this study have not been compensated, because the instruments were run at low filter loading settings. We show the regression between the AE33 instruments and the MAAP in Fig. 11 (the time series is shown in Fig. S9). BC concentrations were higher during the day, showing the contribution of local traffic. During the 2.5 days of the experiment, we observed spectral signatures of k similar to that in Klagenfurt. The regression results for these comparisons and extended comparisons performed in Belgium (Maetz and Peters, 2013) and in the United States (USEPA, 2014) are reported in Table 4. The regression between the Aethalometers AE33 exhibits a higher correlation coefficient than the regression between AE33 and legacy Aethalometers. The comparison of a chosen AE33 to legacy Aethalometers also shows a larger variation in the regression slope than the comparison to the AE33 instruments.
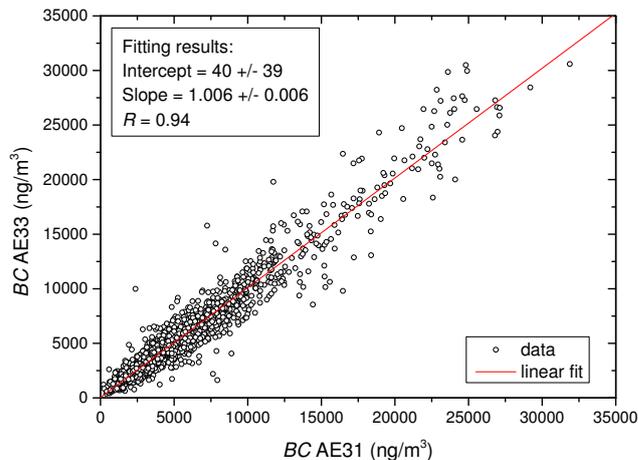
3.7 Cross-sensitivity to scattering

The cross-sensitivity of the Aethalometer AE33 to the scattering particles collected in the filter matrix was tested in a laboratory experiment. Ammonium sulfate aerosols were used as model scattering aerosols. Ammonium sulfate was aerosolized in an atomizer from a solution. The airstream was dried to relative humidity below 30 % by mixing with dry clean air and additionally using diffusion driers. The particles were injected in the mixing chamber (volume $0.5 \, \mathrm{m^3}$). Up to eight outlet ports with equal concentrations distributed
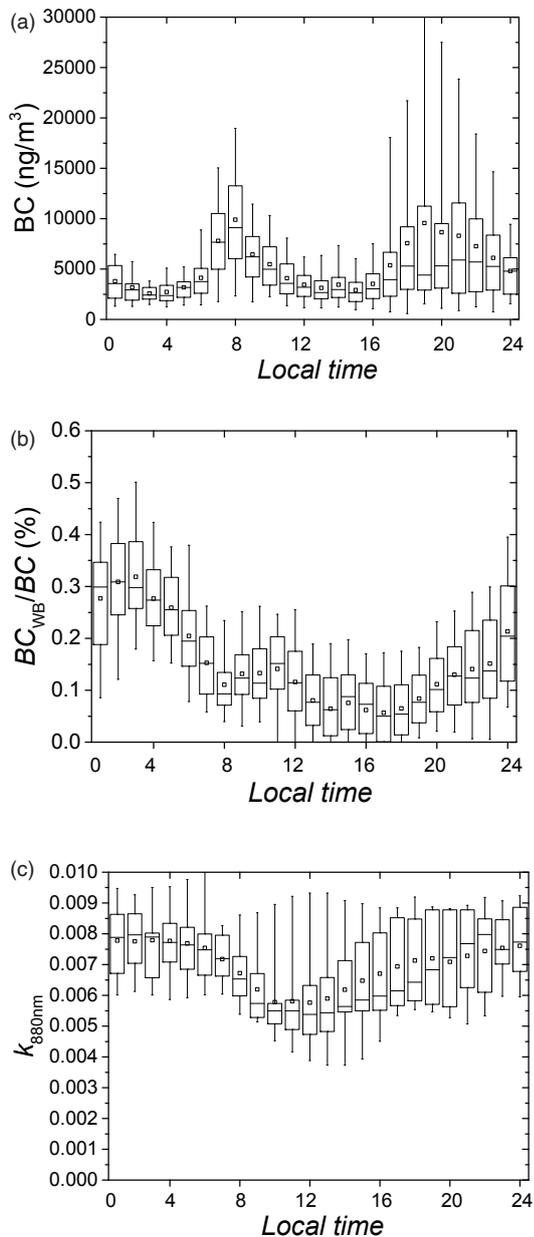
Figure 9. Diurnal plots of **(a)** BC, **(b)** contribution of biomass burning to total BC and **(c)** the compensation parameter k at 880 nm. The analysis was performed for the workdays during the Klagenfurt campaign. The central line represents the group median, the vertical boxes represent data points between the 25th and 75th percentiles; the whiskers represent data points between the 5th and 95th percentiles; the square represents the average value.

Figure 10. Correlation of BC measurements (2 weeks, Klagenfurt, Austria) between the Aethalometers AE31 (using quartz filter) and AE33 (using TFE-coated glass fiber filter), showing 5 min averages of data compensated for the loading effect.
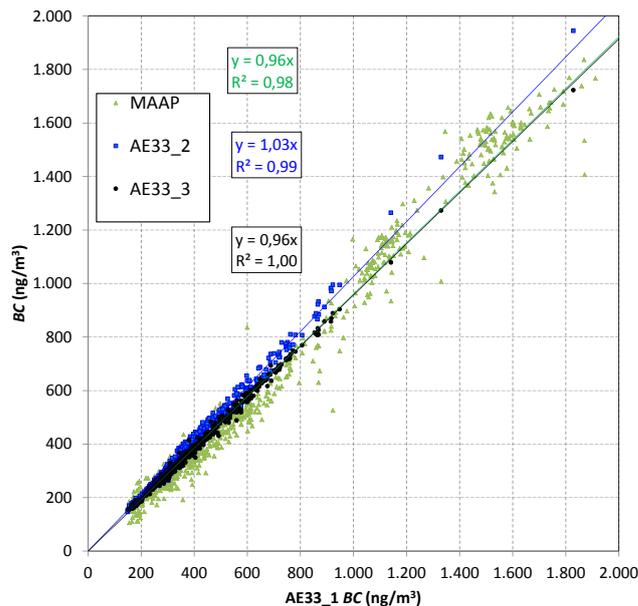
Figure 11. Regression: BC measurements by AE33 and MAAP. The data were resampled to 5 min for both instruments. The Aethalometer AE33 uses measurements at 880 nm and parameters $C = 1.57$ and $\sigma_{air} = 7.77 \, \text{m}^2 \, \text{g}^{-1}$ to obtain BC. The MAAP determines BC at 637 nm using $\sigma_{air} = 6.6 \, \text{m}^2 \, \text{g}^{-1}$; the effective parameter C is not disclosed and is inherent in the instrumental algorithm.

the aerosol to the instrumentation. The scattering coefficient was measured with a polar nephelometer (Aurora 4000, Ecotech Pty Ltd). The truncation error was corrected using the methodology described in Müller et al. (2011b). The loading of the spot with ammonium sulfate was chosen to be higher than what would be expected in most polluted atmo-

spheres encountered in heavily polluted environments. Mass concentrations for the two experiments shown in Fig. 12 were derived from the particle number size distributions and the density of $1.53 \, \text{g cm}^{-3}$ for ammonium sulfate and amount to 39 and $43 \, \mu\text{g m}^{-3}$. The volume mean diameters were measured to be 156 and 257 nm, respectively.
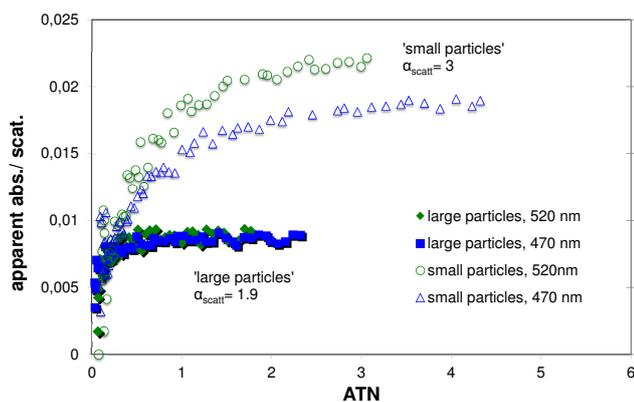
Figure 12. The AE33 instrumental cross-sensitivity to scattering – the ratio of the apparent absorption coefficient and the scattering coefficient as a function of attenuation (ATN).

The sensitivity of the determination of the absorption coefficient from the AE33 to the scattering is shown in Fig. 12, where we plot the ratio of apparent absorption coefficient and the scattering coefficient as a function of ATN. We see two features: firstly, the cross-sensitivity of absorption to scattering is small in the range of below 1 to 1.5 %, smaller than estimated for older Aethalometers (Rosen and Novakov, 1983). Secondly, the cross-sensitivity is almost constant over the whole experimental range and does not depend significantly on ATN. Cross-sensitivity does have some dependence on the size of the absorbing particles. For the PSAP, Nakayama et al. (2010) found a size-dependent sensitivity. We have used absorbing particles of different size to challenge the response of the Aethalometers AE33 and found that C does not depend greatly on the absorbing particle size within the measured range (ACTRIS, 2014b).

4 Conclusions

The filter loading effect hinders optical measurements of black carbon performed by filter-based absorption photometers. This effect can be analyzed using the BC(ATN) method, in which BC as a function of ATN is analyzed. Measurements at various locations and times of the year show big differences in the filter loading effect. In Aethalometers, the loading of the filter spot results in a linear reduction of the instrumental sensitivity. This allows the determination of the amplitude of the loading effect using attenuation measurements from two differently loaded spots – a dual-spot approach. A new real-time loading effect compensation algorithm based on the dual-spot measurements was developed and incorporated in the new Aethalometer model AE33. During a winter measurement campaign in Klagenfurt, Austria, the performance of the new algorithm was compared with the Aethalometer AE31 measurements, which were compensated using the Weingartner et al. (2003) compensation method. The BC(ATN) analyses of the compensated data in-

dicate excellent performance of the new algorithm for all seven measurement wavelengths. Improvements in the determination of the spectral dependence of absorption, as described by the Ångström exponent, allow for real-time high time resolution source apportionment by the AE33. The dual-spot compensation algorithm determines the value of the compensation parameter k with high temporal resolution, which indicates changes in aerosol properties on the daily timescale. As shown during the Klagenfurt and Leipzig campaigns, the performance of the AE33 compares well with the compensated filter photometers of older design and provides forward continuity with data from legacy Aethalometers.

The Supplement related to this article is available online at doi:10.5194/amt-8-1965-2015-supplement.

References

ACTRIS, ACTRIS Intercomparison Workshop for Integrating Nephelometer and Absorption Photometers, http://www.wmo-gaw-wcc-aerosol-physics.org/files/ ACTRIS-intercomparison-workshop-integrating-nephelometer- and-absorption-photometer-02-03-2013.pdf (last access: 1 May 2015), 2014a.

ACTRIS, ACTRIS Workshop on the Reference method for Multi-Wavelength Absorption, http://www.wmo-gaw-wcc-aerosol-physics.org/files/ ACTRIS-Reference-Method-Multi-wavelength-Absorption-03-2013.pdf (last access: 1 May 2015), 2014b.

Ångström, A.: On the atmospheric transmission of sun radiation and on dust in the air, Geogr. Ann., 11, 156–166, 1929.

Arnott, W. P., Moosmüller, H., Rogers, C. F., Jin, T., and Bruch, R.: Photoacoustic spectrometer for measuring light absorption by aerosols: instrument description, Atmos. Environ., 33, 2845–2852, 1999.

Arnott, W. P., Hamasha, K., Moosmuller, H., Sheridan, P. J., and Ogren, J. A.: Towards aerosol light-absorption measurements with a 7-wavelength Aethalometer: evaluation with a photoacoustic instrument and 3-wavelength nephelometer, Aerosol Sci. Tech., 39, 17–29, doi:10.1080/027868290901972, 2005.

Birch, M. E. and Cary, R. A.: Elemental carbon-based method for monitoring occupational exposures to particulate diesel exhaust, Aerosol Sci. Tech., 25, 221–241, 1996.

Bodhaine, B. A.: Aerosol absorption measurements at Barrow, Mauna Loa and the South Pole, J. Geophys. Res.-Atmos., 100, 8967–8975, doi:10.1029/95jd00513, 1995.

Bond, T. C., Anderson, T. L., and Campbell, D.: Calibration and intercomparison of filter-based measurements of visible light absorption by aerosols, Aerosol Sci. Tech., 30, 582–600, doi:10.1080/027868299304435, 1999.

Bond, T. C., Doherty, S. J., Fahey, D. W., Forster, P. M., Berntsen, T., DeAngelo, B. J., Flanner, M. G., Ghan, S., Kärcher, B., Koch, D., Kinne, S., Kondo, Y., Quinn, P. K., Sarofim, M. C., Schultz, M. G., Schulz, M., Venkataraman, C., Zhang, H., Zhang, S., Bellouin, N., Guttikunda, S. K., Hopke, P. K., Jacobson, M. Z., Kaiser, J. W., Klimont, Z., Lohmann, U., Schwarz, J. P., Shindell, D., Storelvmo, T., Warren, S. G., and Zender, C. S.: Bounding the role of black carbon in the climate system: a scientific assessment, J. Geophys. Res.-Atmos., 118, 5380–5552, doi:10.1002/jgrd.50171, 2013.

Cavalli, F., Viana, M., Yttri, K. E., Genberg, J., and Putaud, J.-P.: Toward a standardised thermal-optical protocol for measuring atmospheric organic and elemental carbon: the EUSAAR protocol, Atmos. Meas. Tech., 3, 79–89, doi:10.5194/amt-3-79-2010, 2010.

Chow, J. C., Watson, J. G., Pritchett, L. C., Pierson, W. R., Frazier, C. A., and Purcell, R. G.: The DRI thermal/optical reflectance carbon analysis system: description, evaluation and applications in US air quality studies, Atmos. Environ., 27, 1185–1201, 1993.

Collaud Coen, M., Weingartner, E., Schaub, D., Hueglin, C., Corrigan, C., Henning, S., Schwikowski, M., and Baltensperger, U.: Saharan dust events at the Jungfraujoch: detection by wavelength dependence of the single scattering albedo and first climatology analysis, Atmos. Chem. Phys., 4, 2465–2480, doi:10.5194/acp-4-2465-2004, 2004.

Collaud Coen, M., Weingartner, E., Apituley, A., Ceburnis, D., Fierz-Schmidhauser, R., Flentje, H., Henzing, J. S., Jennings, S. G., Moerman, M., Petzold, A., Schmid, O., and Baltensperger, U.: Minimizing light absorption measurement artifacts of the Aethalometer: evaluation of five correction algorithms, Atmos. Meas. Tech., 3, 457–474, doi:10.5194/amt-3-457-2010, 2010.

Favez, O., El Haddad, I., Piot, C., Boréave, A., Abidi, E., Marchand, N., Jaffrezo, J.-L., Besombes, J.-L., Personnaz, M.-B., Sciare, J., Wortham, H., George, C., and D'Anna, B.: Inter-comparison of source apportionment models for the estimation of wood burning aerosols during wintertime in an Alpine city (Grenoble, France), Atmos. Chem. Phys., 10, 5295–5314, doi:10.5194/acp-10-5295-2010, 2010.

Fialho, P., Hansen, A. D. A., and Honrath, R. E., Absorption coefficients by aerosols in remote areas: a new approach to decouple dust and black carbon absorption coefficients using seven-wavelength Aethalometer data, J. Aerosol Sci., 36, 267–282, 2005.

Grahame, T. J., Klemm, R., and Schlesinger, R. B.: Public health and components of particulate matter: The changing assessment of black carbon, J. Air Waste Manage., 64, 620–660, doi:10.1080/10962247.2014.912692, 2014.

Gundel, L. A., Dod, R. L., Rosen, H., and Novakov, T.: The relationship between optical attenuation and black carbon concentration for ambient and source particles, Sci. Total Environ., 36, 197–202, doi:10.1016/0048-9697(84)90266-3, 1984.

Hansen, A. D. A., Rosen, H., and Novakov, T.: Real-time measurement of the aerosol absoprtion-coefficient of aerosol particles, Appl. Opt., 21, 3060–3062, doi:10.1364/AO.21.003060, 1982.

Hansen, A. D. A., Rosen, H., and Novakov, T.: The aethalometer – an instrument for the real-time measurement of optical absorption by aerosol particles, Sci. Total Environ., 36, 191–196, 1984.

Hansen, A. D. A., Conway, T. J., Steele, L. P. Bodhaine, B. A., Thoning, K. W., Tans, P., and Novakov, T.: Correlations among combustion effluent species at Barrow Alaska: aerosol black carbon, carbon dioxide, and methane, J. Atmos. Chem. 9, 283–299, doi:10.1007/BF00052838, 1989.

Holanda, B. A., Brito, J. F., Barbosa, H. M. J., Andreae, M. O., Saturno, J., Pöhlker, C., Rizzo, L., and Artaxo, P.: Light Absorption of PM$_{2.5}$ and PM10 Biogenic Aerosol Particles in Amazonia measured using several techniques, AGU Fall Meeting, San Francisco, California, USA, 15–19 December 2014, A23A-3197, 2014.

Hyvärinen, A.-P., Vakkari, V., Laakso, L., Hooda, R. K., Sharma, V. P., Panwar, T. S., Beukes, J. P., van Zyl, P. G., Josipovic, M., Garland, R. M., Andreae, M. O., Pöschl, U., and Petzold, A.: Correction for a measurement artifact of the Multi-Angle Absorption Photometer (MAAP) at high black carbon mass concentration levels, Atmos. Meas. Tech., 6, 81–90, doi:10.5194/amt-6-81-2013, 2013.

IPCC, Climate Change 2013: The Physical Science Basis. Contribution of Working Group I to the Fifth Assessment Report of the Intergovernmental Panel on Climate Change, edited by: Stocker, T., Dahe, Q., and Plattner, G.-K., Cambridge University Press, Cambridge, UK and New York, NY, USA, 2013.

Janssen, N. A. H., Hoek, G., Simic-Lawson, M., Fischer, P., van Bree, L., Ten Brink, H., Keuken, M., Atkinson, R. W., Anderson, H. R., Brunekreef, B., and Cassee, F. R.: Black carbon as an additional indicator of the adverse health effects of airborne particles compared with PM$_{10}$ and PM$_{2.5}$, Environ. Health Persp., 119, 1691–1699, doi:10.1289/ehp.1003369, 2011.

Janssen, N. A. H., Gerlofs-Nijland, M. E., Lanki, T., Salonen, R. O., Cassee, F., Hoek, G., Fischer, P., Brunekreef, B., Krzyzanowski, M.: Health effects of black carbon, The WHO European Centre for Environment and Health, Bonn, Germany, World Health Organisation Regional Office for Europe, Copenhagen, Denmark, 2012.

Kirchstetter, T. W., Novakov, T., and Hobbs, P. V.: Evidence that the spectral dependence of light absorption by aerosols is affected by organic carbon, J. Geophys. Res.-Atmos., 109, D21208, doi:10.1029/2004JD004999, 2004.

Maetz, P. and Peters, O.: Comparing Black Carbon monitors as employed by the different measuring networks in Belgium, Monitoring Ambient Air 2013, 10–11 December 2013, London, UK, 2013.

Müller, T., Henzing, J. S., de Leeuw, G., Wiedensohler, A., Alastuey, A., Angelov, H., Bizjak, M., Collaud Coen, M., Engström, J. E., Gruening, C., Hillamo, R., Hoffer, A., Imre, K., Ivanow, P., Jennings, G., Sun, J. Y., Kalivitis, N., Karlsson, H., Komppula, M., Laj, P., Li, S.-M., Lunder, C., Marinoni, A., Martins dos Santos, S., Moerman, M., Nowak, A., Ogren, J. A., Petzold, A., Pichon, J. M., Rodriquez, S., Sharma, S., Sheridan, P. J., Teinilä, K., Tuch, T., Viana, M., Virkkula, A., Weingartner, E., Wilhelm, R., and Wang, Y. Q.: Characterization and intercomparison of aerosol absorption photometers: result of two intercomparison workshops, Atmos. Meas. Tech., 4, 245–268, doi:10.5194/amt-4-245-2011, 2011a.

Müller, T., Laborde, M., Kassell, G., and Wiedensohler, A.: Design and performance of a three-wavelength LED-based total scatter and backscatter integrating nephelometer, Atmos. Meas. Tech., 4, 1291–1303, doi:10.5194/amt-4-1291-2011, 2011b.

Nakayama, T., Kondo, Y., Moteki, N., Sahu, L. K., Kinase, T., Kita, K., and Matsumi, Y.: Size-dependent correction factors for absorption measurements using filter-based photometers: PSAP and COSMOS, J. Aerosol Sci., 41, 333–343, 2010.

Park, S. S., Hansen, A. D. A., and Cho, Y.: Measurement of real time black carbon for investigating spot loading effects of Aethalometer data, Atmos. Environ., 11, 1449–1455, doi:10.1016/j.atmosenv.2010.01.025, 2010.

Petzold, A. and Schönlinner, M.: Multi-angle absorption photometry – A new method for the measurement of aerosol light absorption and atmospheric black carbon, J. Aerosol Sci., 35, 421–441, doi:10.1016/j.jaerosci.2003.09.005, 2004.

Petzold, A., Schloesser, M., Sheridan, P. J., Arnott, W. P., Ogren, J. A., and Virkkula, A.: Evaluation of multi-angle absorption photometry for measuring aerosol light absorption, Aerosol Sci. Tech., 39, 40–51, doi:10.1080/027868290901945, 2005.

Petzold, A., Ogren, J. A., Fiebig, M., Laj, P., Li, S.-M., Baltensperger, U., Holzer-Popp, T., Kinne, S., Pappalardo, G., Sugimoto, N., Wehrli, C., Wiedensohler, A., and Zhang, X.-Y.: Recommendations for reporting "black carbon" measurements, Atmos. Chem. Phys., 13, 8365–8379, doi:10.5194/acp-13-8365-2013, 2013.

Ramanathan, V. and Carmichael, G.: Global and regional climate changes due to black carbon, Nat. Geosci., 1, 221–227, doi:10.1038/ngeo156, 2008.

Rosen, H. and Novakov, T. : Optical transmission through aerosol deposits on diffusely reflective filters: a method for measuring the absorbing component of aerosol particles, Appl. Opt., 22, 1265–1267, doi:10.1364/AO.22.001265, 1983.

Rosen, H., Hansen, A. D. A., Gundel, L., and Novakov, T.: Identification of the optically absorbing component in urban aerosols, Appl. Opt., 17, 3859–3861, 1978.

Sandradewi, J., Prévôt, A. S. H., Weingartner, E., Schmidhauser, R., Gysel, M., and Baltensperger, U.: A study of wood burning and traffic aerosols in an Alpine valley using a multi-wavelength aethalometer, Atmos. Environ., 42, 101–112, 2008a.

Sandradewi, J., Prévôt, A. S. H., Szidat, S., Perron, N., Alfarra, M. R., Lanz, V. A., Weingartner, E., and Baltensperger, U.: Using aerosol light absorption measurements for the quantitative determination of wood burning and traffic emission contributions to particulate matter, Environ. Sci. Technol., 42, 3316–3323, doi:10.1021/es702253m, 2008b.

Sciare, J., Favez, O., Oikonomou, K., Sarda-Estève, R., Cachier, R., and Kazan V., Long-term observation of carbonaceous aerosols in the Austral Ocean: Evidence of a marine biogenic origin, J. Geophys. Res., 114, D15302, doi:10.1029/2009JD011998, 2009.

Segura, S., Estellés, V., Titos, G., Lyamani, H., Utrillas, M. P., Zotter, P., Prévôt, A. S. H., Močnik, G., Alados-Arboledas, L., and Martínez-Lozano, J. A.: Determination and analysis of in situ spectral aerosol optical properties by a multi-instrumental approach, Atmos. Meas. Tech., 7, 2373–2387, doi:10.5194/amt-7-2373-2014, 2014.

Stephens, M. , Turner, N., and Sandberg, J.: Particle Identification by Laser-Induced Incandescence in a Solid-State Laser Cavity, Appl. Opt., 42, 3726–3736, 2003.

USEPA – U.S. Environmental Protection Agency and Battelle Memorial Institute, Environmental Technology Verification Report, Magee Scientific Model AE33 Aethalometer, Battelle, Columbus, Ohio, USA, February 2014, http://cfpub.epa.gov/si/si_public_file_download.cfm?p_download_id=520219 (last access: 1 May 2015), 2014.

Virkkula, A.: Correction of the Calibration of the 3-wavelength Particle Soot Absorption Photometer (3 PSAP), Aerosol Sci. Tech., 44, 706–712, doi:10.1080/02786826.2010.482110, 2010.

Virkkula, A., Ahlquist, N. C., Covert, D. S., Arnott, W. P., Sheridan, P. J., Quinn, P. K., and Coffman, D. J.: Modification, calibration and a field test of an instrument for measuring light absorption by particles, Aerosol Sci. Tech., 39, 68–83, doi:10.1080/027868290901963, 2005.

Virkkula, A., Mäkelä, T., Hillamo, R., Yli-Tuomi, T., Hirsikko, A., Hämeri, K., and Koponen, I. K.: A simple procedure for correcting loading effects of aethalometer data, J. Air Waste Manage., 57, 1214–1222, doi:10.3155/1047-3289.57.10.1214, 2007.

Wehner, B. and Wiedensohler, A.: Long term measurements of submicrometer urban aerosols: statistical analysis for correlations with meteorological conditions and trace gases, Atmos. Chem. Phys., 3, 867–879, doi:10.5194/acp-3-867-2003, 2003.

Weingartner, E., Saathoff, H., Schnaiter, M., Streit, N., Bitnar, B., and Baltensperger, U.: Absorption of light by soot particles: determination of the absorption coefficient by means of aethalometers, J. Aerosol Sci., 34, 1445–1463, doi:10.1016/S0021-8502(03)00359-8, 2003.

WMO/GAW Aerosol Measurement Procedures: Guidelines and Recommendations. TD No. 1178, September 2003.

Yang, M., Howell, S. G., Zhuang, J., and Huebert, B. J.: Attribution of aerosol light absorption to black carbon, brown carbon, and dust in China – interpretations of atmospheric measurements during EAST-AIRE, Atmos. Chem. Phys., 9, 2035–2050, doi:10.5194/acp-9-2035-2009, 2009.